THE BULLETIN OF OKAYAMA UNIVERSITY OF SCIENCE No. 43 A pp. 17-25(2007)

Contracted-Independent-Electron-Model study of multiple ionization of atoms by swift ion impacts

Toshiaki KANEKO and Takao WADA
Graduate School of Science, Okayama University of Science
1-1 Ridai-cho, Okayama 700-0005, Japan
(Received October 1, 2007; accepted November 2, 2007)

Multiple ionization process of target atoms induced by swift ions was investigated on the basis of the Contracted Independent Electron Model (CIEM) with the use of the successive ionization potentials. The modeled the impact-parameter-dependent ionization probability satisfies a scaling law and, then, is implicitly proved not to be over unity even for the incidence of highly charged ions. We also studied comprehensively the multiple ionization process together with other models. A comprehensive study shows that the CIEM yields better agreement than other models with the experimental results for He, Ne and Ar targets bombarded by the MeV/amu ions.

Keywords: collision; multiple ionization; independent electron model; energy-loss.

1. Introduction

Since ion accelerators were widely applied to the investigation of ion-material interaction, ionization has been one of the important fundamental processes in atomic collision phenomena [1,2]. As to the multiple ionization of a target, intensive researches have been done especially since about twenty years ago [3-11]. Those researches were focused on the two electron system of a helium target and a hydrogen molecule target. The investigations have been extended to many electron systems as noble gas targets[12,13], hetero molecule targets and fullerene targets. There are some cases where multiple ionization process accompanies the electron-capture and/or electron-loss processes.

Regarding the one-electron ionization of light-gas targets, the first-order theories [14] have been successfully applied. Another method often used in analysis is the classical binary encounter model [15]. As for the double ionization in a two-electron system, the interference in the excitation amplitude between the shake-off process and the two-step process results in the difference in the ionization cross section induced by the proton impact and by the anti-proton impact. Generally speaking, in a many-electron system it is so hard to explicitly take into account the electron correlation. Therefore the statistical models have been developed. So far two models were well known. One is the statistical energy-deposition model(SEDM) [16]. This model has been employed together with the impact-parameter-dependent energy deposition [3-5,17]. Though it is a pioneering work, the key factor, relating to the transition matrix element (we call g-factor), is a pure fitting parameter in practical use. So any quantitative dependences of the probability on physical parameters, are not clear. In fact, the magnitude of the g-factor varies over a wide range and case by case, as $g = 0.005 - 0.1$ [3-5] and $g = 1$ [17]. Another model is the independent electron model (IEM). This is based on the single-electron ionization probability $P(b)$ as a function of impact-parameter b [12,18]. Regarding the ionization and the related energy-loss phenomena, there have been a number of theories based on the impact-parameter treatment [19]. However, except for ions with a relatively low charge, the probability $P(b)$ tends to be over unity, judging from the scaling law [20]. In order to avoid this demerit, there are several compulsory prescriptions [12].

Cocke[17] measured the recoil-ion charge-state spectra in collisions of the 25-45 MeV chlorine ions with He, Ne, and Ar targets. In this analysis, he used the conventional IEM, or, the binomial distribution together with $P(b)$ values obtained by Olson[21] in the Classical-Trajectory Monte Carlo (CTMC) calculation. He also compared with the result of the SEDM under taking $g=1$.

Recently, we proposed the model, which was well applied to multiple ionization of diatom molecule targets [22] and the fullerene target [23]. The purpose of this paper is to show the results on multiple ionization study of single-atom targets. In addition we also show the comprehensive results, obtained from the other models. Through this paper, m, e and $\hbar$ denote, respectively, the electron rest mass, the elementary charge, and the Planck constant divided by 2π. In addition, we use the Bohr radius $a_0=\hbar^2/me^2$=0.0529nm and the Bohr speed $v_0=e^2/\hbar$=2.19×10^6 m/s.

2. Theoretical models

2.1 Contracted Independent Electron Model (CIEM)

In the conventional independent electron model (IEM), the ionization potential value is common to all of the electrons in a shell. However, we think that the more the degree of ionization is growing up, the more scarcely a further ionization will take place. Namely, as the degree of ionization is promoted, the binding energy of the residual electrons increases. In other words, the residual electron cloud will be bound on the ion more strongly and tend to be contracted a bit. In this sense we call 'the contracted IEM(CIEM)'. Let us assume n electrons to be ionized among N equivalent electrons in a shell. The b-dependent ionization probability for the single electron ionization $P_1^N(b)$ is proportional to ${}_NC_1P(b,\varepsilon_1)[1-P(b,\varepsilon_2)]^{N-1}$. The first factor denotes the binomial coefficient, and the second is the ionization probability of a single electron in the energy state ε_1. The third means the probability that the residual $N-1$ electrons in the post-ionizing state ε_2, will not be ionized further. Thus, by using the i-th ionization potential energy ε_i (i=1,2,..,N), the ionization probabilities $P_n^N(b)$ ($n=0,1,2,\cdots,N$) for the n-fold ionization process is determined as

$$P_0^N(b)=\frac{1}{D}[1-P(b,\varepsilon_1)]^N,\quad P_n^N(b)=\frac{1}{D}{}_NC_n\prod_{i=1}^{n}P(b,\varepsilon_i)[1-P(b,\varepsilon_{n+1})]^{N-n},$$

where $P_0^N(b)$ is the probability for no-ionization taking place, and the factor D denotes the normalization constant, determined by satisfying $\Sigma_{n=0}^{N}P_n^N(b)=1$. The reason of introducing the factor D is that the final states of the residual (not ionized) electrons is assumed to depend on the number of electrons. Namely, the final state wavefunctions for those electrons are not orthogonal. The corresponding multiple ionization cross sections are obtained by

$$\sigma_n^N=2\pi\int_0^\infty db\,b\,P_n^N(b).$$

In the above expression, the creation of inner-shell holes is neglected. We remark that if we set all of ε_i to be the same as ε, one can find that $D=1$ and the CIEM probabilities reduces to the IEM ones. This method can be straightforwardly extended to multi-shell systems.

2.2 Modeled Ionization probability $P(b,\varepsilon)$

Here we adopt a hydrogen-like model, where the active electron is characterized by the effective charge Z_e and the orbital-size parameter $a=a_0/Z_e$, determined by $Z_e=(2\hbar^2\varepsilon/me^4)^{1/2}$. Let us consider the single electron ionization process of the active electron, bombarded by a swift ion with a charge Z_1e and a speed v relative to the electron in the Born approximation. According to a quantum-mechanical treatment [24], the differential ionization cross section for the electron is given by the following reduced form:

$$\frac{d^2\sigma_{ion}}{dKdQ} = 8\pi a_0{}^2 \left(\frac{Z_1 v_0}{Z_e v}\right)^2 \frac{K}{Q} \frac{2^8 \exp\left(-\frac{2}{K}\arctan\frac{2K}{1-K^2+Q^2}\right)}{\left[1+(K+Q)^2\right]^3\left[1+(K-Q)^2\right]^3} \frac{Q^2+(1+K^2)/3}{1-\exp(-2\pi/K)} \quad .$$

Here, we introduced the non-dimensional wavenumber K of ionized electron, and the non-dimensional momentum transfer Q. Hereby we have the expression for the differential ionization cross section per unit interval of K as

$$\frac{d\sigma_{ion}}{dK} = \int_{Q_{\min}(K)}^{Q_{\max}} dQ \frac{d^2\sigma_{ion}}{dKdQ} \quad ,$$

where $Q_{\min}(K) = (K^2+1)/(2V)$, $Q_{\max} = 2\mu V/m$, $V = v/(Z_e v_0)$ and μ is the reduced mass.

In order to model the ionization probability even for highly charged projectiles, we adopt the classical picture of the energy transfer to the electron. In Rutherford picture, the energy transfer $\Delta E(b)$ from a projectile with charge $Z_1 e$ and speed v to the electron is given as a function of impact parameter b [25] by

$$\Delta E(b) = \frac{2Z_1{}^2 e^4}{mv^2} \frac{1}{b^2 + (Z_1 e^2/mv^2)^2} \quad .$$

Here the excited electron is initially bound to the nucleus so that impact parameter b in the above expression is equivalent to that of the projectile in the conventional meaning. Next, let us introduce $\Delta E(b)$ into the ionization. Since the binding effect is neglected, we are allowed to regard $\Delta E(b)$ as the kinetic energy $(\hbar k)^2/(2m)$ of the ionized electron. Then, the wavenumber k of the ionized electron is expressed as a function of b. We define $K(b) = ka = (2mva/\hbar)A/\sqrt{A^2+b^2}$ with $A = Z_1 e^2/mv^2$, and $P(b,\varepsilon)$ is requested to derive σ_{ion}. Then, we finally obtain the ionization probability as a function of impact parameter as

$$P(b,\varepsilon) = K(b)^4 \int_{Q_{\min}(K(b))}^{Q_{\max}} \frac{dQ}{Q} \frac{Q^2+(1+K(b)^2)/3}{1-\exp(-2\pi/K(b))} \frac{2^8 \exp\left(-\frac{2}{K(b)}\arctan\frac{2K(b)}{1-K(b)^2+Q^2}\right)}{\left[1+(K(b)+Q)^2\right]^3\left[1+(K(b)-Q)^2\right]^3} \quad ,$$

where the ε-dependence appears in $K(b)$ through the orbital parameter a. One can confirm that the above equation actually reproduces σ_{ion}, which is equivalent to the quantum-mechanical coulomb-Born ionization cross section, except for the upper limit in the K-integral. However, this difference is of no importance as far as the speed is not so small.

2.3 Scalings of $P(b,\varepsilon)$ and σ_{ion}

Here we derive the scaling laws for $P(b,\varepsilon)$ and σ_{ion}. In order to make clear the dependences on the physical parameters, we denote $P(b,\varepsilon)$ as $P(b,v,Z_1,Z_e)$. It is convenient to define the reduced impact parameter $\tilde{b} \equiv Z_e{}^2 b/Z_1$ and the reduced speed $\tilde{v} \equiv v/Z_e$ Then we have $K(b) = 2ma_0\tilde{v}/\hbar \times \tilde{A}/\sqrt{(\tilde{A})^2+\tilde{b}^2} \equiv K(\tilde{b})$, $\tilde{A} = e^2/(m\tilde{v}^2)$, $Q_{\min}(K(\tilde{b})) = [K(\tilde{b})^2+1](v_0/2\tilde{v})$, $Q_{\max} = 2(\tilde{v}/v_0)(\mu/m)$. Then after simple algebra, we can prove the scaling rule

$$P(b,v,Z_1,Z_e) = P(\tilde{b},\tilde{v},1,1)$$

Here $P(\tilde{b},\tilde{v},1,1)$ means the ionization probability of a hydrogen atom in collision with an incident proton moving at a speed $\tilde{v}$ along a straight-line trajectory at an impact parameter $\tilde{b}$. This scaling law guarantees that $P(b,v,Z_1,Z_e)$ is not over unity for any Z_1, as far as $P(\tilde{b},\tilde{v},1,1)$ does not exceed unity. If we write the corresponding ionization cross section as $\sigma_{ion} \equiv \sigma_{ion}(v,Z_1,Z_e)$, one immediately finds

$$\sigma_{ion}(v,Z_1,Z_e) = (Z_1/Z_e{}^2)^2 \sigma_{ion}(\tilde{v},1,1) \quad , \quad \sigma_{ion}(\tilde{v},1,1) = 2\pi \int_0^\infty d\tilde{b}\, \tilde{b}\, P(\tilde{b},\tilde{v},1,1) .$$

For comparison, we show that the b-dependent SCA ionization probability $P^{SCA}(b,v,Z_1,Z_e)$ and the corresponding cross section $\sigma_{ion}^{SCA}(v,Z_1,Z_e)$ can be scaled [20] as

$$P^{SCA}(b,v,Z_1,Z_e)=(Z_1/Z_e)^2 P^{SCA}(Z_e b, v/Z_e,1,1) \quad , \quad \sigma_{ion}^{SCA}(v,Z_1,Z_e)=(Z_1/Z_e{}^2)^2\sigma_{ion}^{SCA}(\tilde{v},1,1).$$

It is remarkable that except for the prefactor, the SCA scaling relations are only characterized by the orbital effective charge Z_e, whereas in our case both Z_1 and Z_e are both involved in $\tilde{b}$. On the other hand, the present and the SCA cross sections are both scaled in the same scaled form, though the scaling variables of $P(b,\varepsilon)$ are different from the SCA treatment. Finally, we point out the very important aspect that the $P(b,\varepsilon)$ in the SCA grows up as $Z_1{}^2$, resulting in being over unity for a large Z_1 especially at a small b. On the contrary, in our case the prefactor of the scaled probability is just unity and independent of Z_1 so that $P(b,\varepsilon)$ is not over unity even for a large Z_1 over the whole range of b. Therefore the present $P(b,\varepsilon)$ does not request any artificial prescription as the perturbative (or Born) treatments.

3. Numerical results and discussion

First we present the result on the basic quantity $P(b,\varepsilon)\equiv P(b,v,Z_1,Z_e)$. Figure 1 shows the $P(b,\varepsilon)$ as a function of b for the incident ions with $Z_1=1$ (solid line), 3(dash-dot-dot line), 10(dash-dot line) and 20(dashed line) at the impact energy of 1.0 MeV/u (i.e. $v=6.3v_0$), ionizing the target electron of $\varepsilon=0.5(a.u.)$ (i.e. $Z_e=1$). One finds the following features:(1)The $P(b,\varepsilon)$ values do not exceed unity even for large Z_1 values, (2) As the Z_1 value increases, the profile of $P(b,\varepsilon)$ becomes broad with keeping the maximum value about unity, (3)As far as the large-b region is concerned, the $P(b,\varepsilon)$ has an asymptotic form of $1/b^4$, and the overall feature of the $P(b,\varepsilon)$ curve is very similar, independent of Z_1. The asymptotic b^{-4}-dependence can be clearly explained by the asymptotic behavior of $K(b)\approx 1/b$, since the value of the integral in $P(b,\varepsilon)$ is saturated to be a constant at a large b. The solid squares denote the SCA results for $Z_1=1$ [20].

Figure 2 displays the universal trend of the profiles of $P(\tilde{b},\tilde{v},1,1)$ as a function of $\tilde{b}$ for the cases of $\tilde{v}/v_0=0.8$ (dash-dot-dot line), 1(solid line), 3(dashed line), 5(dotted line), and 10(dash-dot line). For the cases of $\tilde{v}/v_0=0.8$ and 1, these curves have a maximum around $\tilde{b}=1.8$ and 1, respectively, while in other cases the $P(\tilde{b},\tilde{v},1,1)$ curves fall off monotonously with increasing $\tilde{b}$. These curves present two features. For a small $\tilde{v}$ less than unity, the width of the curve does not change so much and the absolute values are increasing as $\tilde{v}$ increases. On the other hand, for a large $\tilde{v}$ greater than unity, the maximum value of $P(\tilde{b},\tilde{v},1,1)$ attains to be unity and its width becomes narrower, as $\tilde{v}$ increases. Figure 3 shows the scaled ionization cross section $\sigma_{ion}(\tilde{v},1,1)$ as a function of $\tilde{v}$. The curve becomes maximum at $\tilde{v}=v_0$. We can find this reason straightforwardly from the behavior of $P(\tilde{b},\tilde{v},1,1)$. As is shown in fig.2, in the region of $\tilde{v}>v_0$, the width of the half-maximum of $P(\tilde{b},\tilde{v},1,1)$ becomes narrower. On the other hand, in the region of $\tilde{v}<v_0$, the maximum value of $P(\tilde{b},\tilde{v},1,1)$ becomes smaller with decreasing $\tilde{v}$, while the width of the $P(\tilde{b},\tilde{v},1,1)$ does not change so much. These behaviors of $P(\tilde{b},\tilde{v},1,1)$ clearly explain the reduction of $\sigma_{ion}(\tilde{v},1,1)$ in the regions of $\tilde{v}<v_0$ and $\tilde{v}>v_0$. We would like to remark that the scaled cross section $\sigma_{ion}(\tilde{v},1,1)$ is almost equivalent to the Born ionization cross section for a hydrogen atom bombarded by a proton ($Z_1=1$) at a speed $\tilde{v}$.

Next, we show the results on the Multiple ionization cross section First we display the b-dependent ionization probabilities in the CIEM. Figure 4 shows the multiple ionization probabilities of the Ar target, bombarded by the 1.05 MeV/amu Ar^{4+} ion. Here, one finds that the maximum value of $P_1(b)$ is about 0.61 at $b=1.74\,a_0$. Let us define b_n at which the $P_n(b)$ value becomes maximum. Then the larger the degree of ionization grows up, the smaller the b_n becomes. Namely, the window of the reaction channel of multiple ionization tends to shift inner and inner with increasing n. Thus the ionization window is found to shift towards the nucleus with increasing recoil charge state. Figure 5 shows the multiple ionization cross sections σ_n $(n=1-8)$ of an Ar atom by the 1.05 MeV/u Ar^{q+} $(q=4,6,8,10,12,14)$ impact. In general, it is known that in the multiple ionization process there exist two components, i.e., the charge transfer component and

the direct ionization component. Tonuma et al.[6] eliminated the charge transfer component from the total multiple ionization cross sections with the use of the compound-atom model by Meron and Rosner[26]. Therefore we believe their data refer only to the direct ionization process. Later, for elaboration we will make a comparison with the experimental data by another group. In figure 5(a) and 5(b), the solid and the open symbols refer to the CIEM and the experimental results, respectively, for equivalent q values. In figure 5(a), one finds the squares(q=4), the triangles(q=6), and the circles(q=8), and in fig.5(b) the squares(q=10), the triangles(q=12), and the circles(q=14). The solid and the dashed lines are drawn only to guide the eyes. In the cases of q=4 and 6, the CIEM values are greater than the data for $n \geq 3$. Except for such a deviation, the CIEM results agree well with the data over the wide range of n. Especially, agreement is quite well in the cases of $q \geq 8$.

For a comprehensive study, we calculated the σ_n for the 1.05 MeV/u Ar^{q+} ($q = 4,6,8$) ion impinging on Ar target in the conventional IEM, shown in fig.6, and in the SEDM, shown in fig.7. In fig.6, we use the Hartree-Fock orbital energies E_{3p}=16.08 eV, E_{3s}=34.74 eV[27]. The number of electrons occupied in those shells are assumed to be six and two, respectively. In figure 6, it is very clear that except for $n = 1,2$, the n-dependence of σ_n in the IEM greatly deviates from the experimental data for all cases of $q = 4-8$ considered here. Though we do not show a figure here, we confirmed that the cases of $q = 10-14$ also present the n-dependence of σ_n quite similar to the cases of $q = 4-8$. These features lead us to a conclusion that the conventional IEM represents a poor agreement with the data than the CIEM as far as the derived expression for $P(b,\varepsilon)$ is employed. On the other hand, in fig.7, the total deposited energy by the projectile is calculated on the basis of the local electron density model as a function of b. In order to treat the SEDM in a refined version, we include the energy straggling in the calculation. Here we took the same value of $g = 0.01$ as Kabachnik et al.[3] adopted in their analysis, in order to see how their choice works well. In fig.7, the calculated σ_n in the case of $q = 4$ looks very nice agreement with the data over the range of n considered. In the cases of $q = 6$ and 8, however, agreement with the data is limited at best only for $n \geq 4$. In addition, in these cases, the ionization cross sections for n=1 and 2 are too much lower than the data, and the q-dependence of σ_n is too much weaker than the data. These two tendencies are more strongly confirmed in the cases of q=10-14. In other words, σ_n for n=1-3 is almost independent of q, and the n-dependence of σ_n are far from agreement with the experimental data. According to our experience, the suppression of the SEDM σ_n at a small n seems to be a general trend, and the reduction of g value gives rise to suppression of σ_n at a large n.

We would like to give two comments on the SEDM. The first comment is that the introduction of the energy straggling plays two roles. One role is to change the abrupt vanishing of $P_1(b)$ at a critical b to the smooth vanishing. If the straggling of the energy transfer is ignored, there exists a critical value b_c (see figure 10 of ref.17) beyond which $P_1(b)$ vanishes. This is because at any b beyond b_c the transferred energy is not an amount enough to ionize the electron. Introduction of energy straggling smears out this critical nature. The other role is to enlarge the ionization cross sections for the higher recoil-charge(n) states. We also remark that in spite of the former role, the cross section σ_n for a smaller n is not almost affected by the energy straggling. The second comment is that the choice of g-value in RM theory[16] drastically changes the recoil-charge dependence of the cross section σ_n especially for higher n. On the contrary, σ_n for the case of n=1 cannot be affected significantly.

Up to here, we compared the CIEM results with the experimental data obtained by one group. In order to confirm further, we also compare our results with the data by other experimental group and by another theoretical model[13]. Figure 8 shows the σ_n against the recoil charge state n of the Ar target atom under the incidence of the 1.4 MeV/u Fe^{q+} ($q = 12,15,20$) and U^{44+} ions. Here the solid squares and open circles denote, respectively, the CIEM results and the experimental data[13]. In addition, the thick solid lines denote the CTMC result[13]. In the figure, only the direct ionization component are drawn. At a glance, our results represent the n-dependence of σ_n, which shows rather good agreement and looks better than the CTMC results. The CIEM is found to yield the consistent n-dependence even for the case of the highest incident

charge (44+).

In conclusion, we investigated the multiple ionization process on the basis of the contracted independent electron model. By introducing the energy transfer to the electron, the ionization probability does not implicitly exceed unity even for highly charged ions. Our model of the energy transfer is to take into account the situation that the bound electron will be released from the initial binding and controlled by the electric field induced by a highly charged incident ion. The classical energy-loss approach allows us to include a non-perturbative effect of highly charged ions on the ionization probability. With the use of the modeled ionization probability, comprehensive study was performed on the multiple ionization of atoms in the present model and also in other available models (i.e., IEM, SEDM, and CTMC). Compared with the existing experimental data, the CIEM calculation is found to yield better agreement than other models. Recently, this CIEM model was successfully applied to the diatom-molecular targets [22] and the C_{60} targets [23], and we also obtained good agreement with the experimental data.

Acknowledgement

The authors would like to thank Dr. H. Shibata of the University of Tokyo for informing us of the works of his group on multiple ionization process. They also thank Prof. A. Itoh of Kyoto University, Prof. N. Matsunami of Nagoya university, and Prof. Y. Kido of Ritsumeikan University for useful discussion. One of the authors (T.K.) is grateful for a partial support of a Grant-in-Aid for Scientific Research (C) from the Japan Society for the Promotion of Science(JSPS). This work is also supported by the Academic Frontier Projects by the Ministry of Education, Culture, Sports, Science and Technology(MEXT).

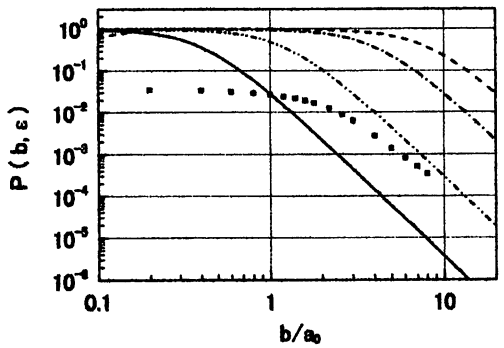

Fig. 1. $P(b,\varepsilon)$ vs b for $\varepsilon = 0.5\,a.u.$ at incident energy of 1.0 MeV/u : the solid line ($Z_1 = 1$), the dash-dot-dot line($Z_1 = 3$), the dash-dot line ($Z_1 = 10$), and the dashed line($Z_1 = 20$). The solid squares denote the SCA results [20].

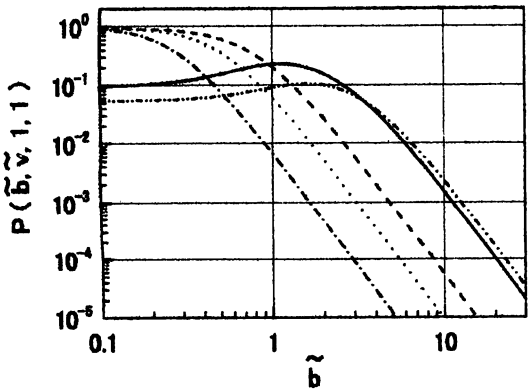

Fig. 2. $P(\tilde{b},\tilde{\nu},1,1)$ vs $\tilde{b}$: the dash-dot-dot line ($\tilde{\nu} = 0.8\nu_0$), the solid line ($\tilde{\nu} = \nu_0$), the dashed line ($\tilde{\nu} = 3\nu_0$), the dotted line ($\tilde{\nu} = 5\nu_0$), and the dash-dot line($\tilde{\nu} = 10\nu_0$).

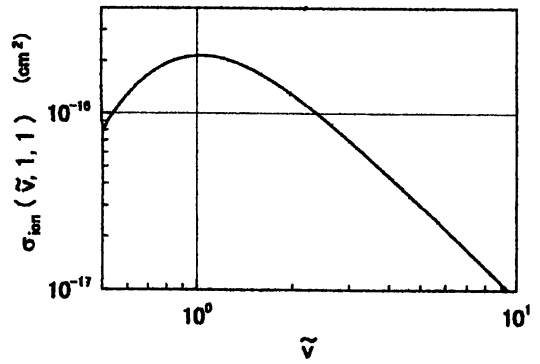

Fig. 3. $\sigma_{ion}(\tilde{v},1,1)$ vs $\tilde{v}$.

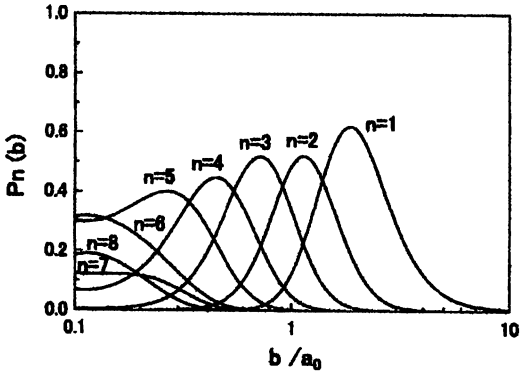

Fig. 4. $P_n(b)$ $(n=1-8)$ vs b for Ar atom by the 1.05 MeV/u Ar^{4+} ion impact in the CIEM calculation. Each value of n is written near the curve.

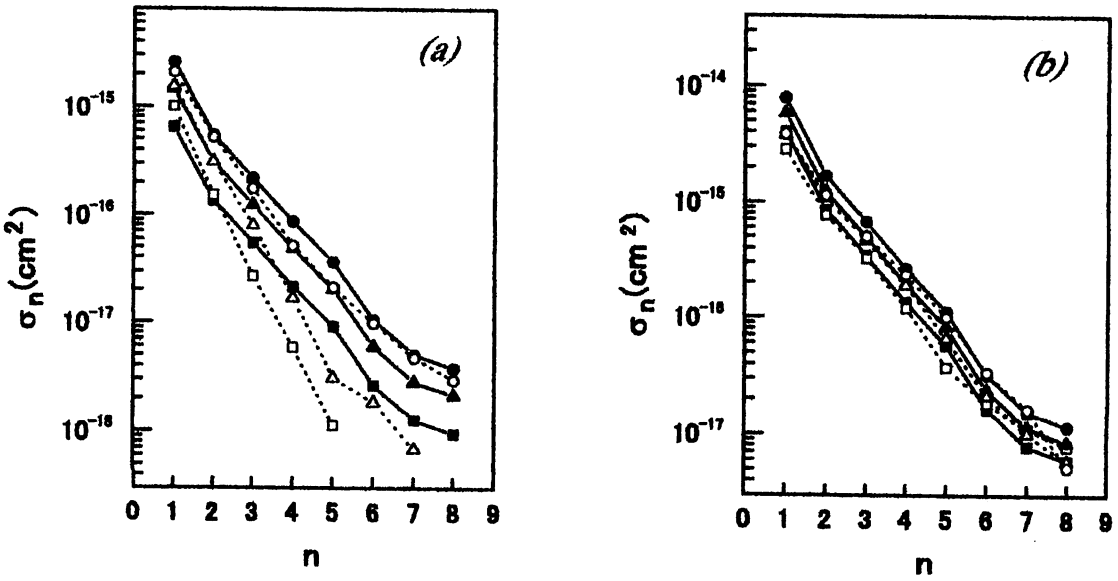

Fig. 5. $\sigma_n(n=1-8)$ vs n for Ar atom by the 1.05 MeV/u $Ar^{q+}(q=4-14)$ ion impact. Solid symbols refer to the CIEM calculation, and open symbols refer to the experimental data [6]. (a) squares($q=4$), triangles($q=6$), and circles($q=8$), (b) squares ($q=10$), triangles($q=12$), and circles($q=14$).

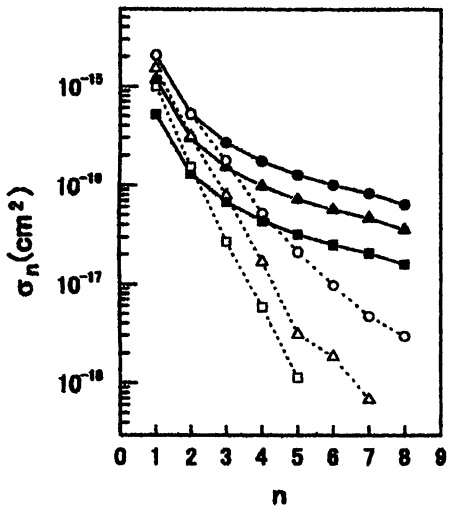

Fig. 6. $\sigma_n(n=1-8)$ vs n for Ar atom by the 1.05 MeV/u $Ar^{q+}(q=4-8)$ ion impact. Solid symbols refer to the IEM calculation, and open symbols refer to the experimental data[6]: squares ($q=4$), triangles ($q=6$), circles ($q=8$).

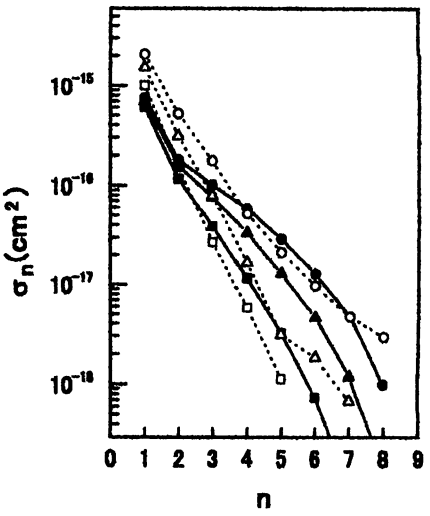

Fig. 7. $\sigma_n(n=1-8)$ vs n for Ar atom by the 1.05 MeV/u $Ar^{q+}(q=4-8)$ ion impact. Solid symbols refer to the SEDM calculation ($g=0.01$), and open symbols refer to the experimental data[6] : squares ($q=4$), triangles ($q=6$), circles($q=8$).

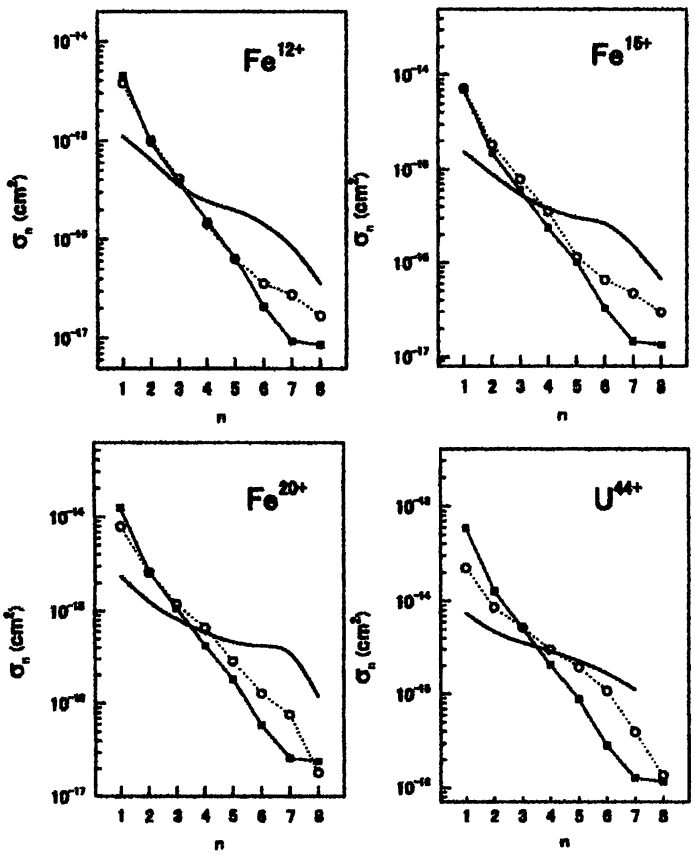

Fig. 8. $\sigma_n(n=1-8)$ vs n for Ar atom bombarded by the 1.4 MeV/u $Fe^{12+,15+,20+}$ and U^{44+} ions. Solid squares connected by thin solid lines refer to the CIEM calculation, and open circles connected by dotted lines refer to the experimental data [13]. Thick solid lines indicate the CTMC result [13].

References

[1] N. Bohr, K. Dan.Vidensk.Selsk.Mat.-Fys.Medd. **18**, no.8 (1948).

[2] E. W. McDaniel, J. B. A. Mitchell, M. E. Rudd, *Atomic Collisions-heavy particle projectiles* (John Wiley and Sons, Inc., 1993).

[3] N. M. Kabachnik, V. N. Kondratyev, Z. Roller-Lutz, and H. O. Lutz, Phys. Rev. A **56**, 2848 (1997).

[4] N. M. Kabachnik, V. N. Kondratyev, Z. Roller-Lutz, and H. O. Lutz, Phys. Rev. A **57**, 990 (1998).

[5] A. Reinkoster, U. Werner, N. M. Kabachnik, and H. O. Lutz, Phys. Rev. A **64**, 23201 (2001).

[6] T. Tonuma, H. Kumagai, T. Matsuo, and H. Tawara, Phys. Rev. A **40**, 6238 (1989).

[7] T. Tonuma, T. Matsuo, M. Kase, T. Kambara, H. Kumagai, S. H. Be, I. Kohno, and H. Tawara, Phys. Rev. A **36**, 1941 (1987).

[8] H. Tawara, T. Tonuma, H. Kumagai, and T. Matsuo, Phys. Rev. A **41**, 116 (1990).

[9] T. Matsuo, T. Tonuma, H. Kumagai, and H. Tawara, Phys. Rev. A **50**, 1178 (1994).

[10] H. Tawara, T. Tonuma, H. Shibata, M. Kase, T. Kambara, S.H.Be, H.Kumagai, and I. Kohno, Phys. Rev. A **33**, 1385 (1986).

[11] M. Saito, Y. Haruyama, N. Hamamoto, K. Yoshida, A. Itoh, and N. Imanishi, J. Phys. B **28**, 5117 (1995).

[12] I. Ben-Itzhak, T. J. Gray, J. C. Legg, and J. H. McGuire, Phys. Rev. A **37**, 3685 (1988).

[13] A. Mueller, B. Schuch, W. Groh, E. Salzborn, H. F. Beyer, P. H. Mokler, and R. E. Olson, Phys. Rev. A **33**, 3010 (1986).

[14] G. H. Gillespie, Phys.Rev. A **18**, 1967 (1978).

[15] L. Vriens, Proc.Roy.Soc. **90**, 935 (1967).

[16] A. Russek and J. Meli, Physica **46**, 222 (1970).

[17] C. L. Cocke, Phys. Rev. A **20**, 749 (1979).

[18] J. H. McGuire and L. Weaver, Phys.Rev. A **16**, 41 (1977).

[19] for example, H. Esbensen and J. A. Golovchenko, Nucl. Phys. A **298**, 382 (1978).

[20] J. M. Hansteen, O. M. Johnsen, and L. Kocbach, At. Data Nucl. Data Tables, **15**, 305 (1975);
J. M. Hansteen and O. P. Mosebekk, Phys.Rev.Lett. **29**, 1361(1972).

[21] R. Olson, J. Phys. B **12**, 1843 (1979).

[22] T. Wada and T. Kaneko, J.Phys.Soc.Jpn. **74**, 568 (2005).

[23] T. Wada and T. Kaneko, J.Phys.Soc.Jpn. **74**, 918 (2005).

[24] L. D. Landau and E. M. Lifshitz, *Quantum Mechanics*(non-relativistic theory), third edition(Pergamon Press,1977)

[25] J. D. Jackson, *Classical Electrodynamics*,second edition(John Wiley and Sons, 1975)Chap.13.

[26] M. Meron and B. Rosner, Phys. Rev. A **30**, 132 (1984).

[27] E. Clementi and C. Roetti, At. Data Nucl. Data Tables, **14**, 177 (1974).